magnetochemistry

MDPI

Article

Dynamic Bloch Chirality and Enhanced Velocities from Spin-Orbit Torque Driven Domain Wall Motion in Thick Magnetic Films

Trae Lawrence Staggers and Shawn David Pollard *

Department of Physics and Materials Science, University of Memphis, Memphis, TN 38152, USA
* Correspondence: shawn.pollard@memphis.edu

Abstract: Spin-orbit torque (SOT) driven domain wall motion has attracted significant attention as the basis for a variety of spintronic devices due to its potential use as a high speed, low power means to manipulate the magnetic state of an object. While most previous attention has focused on ultrathin films wherein the material thickness is significantly less than the magnetic exchange length, recent reports have suggested unique dynamics may be achieved in intermediate and high thickness films. We used micromagnetic modelling to explore the role of the vertically non-uniform spin textures associated with the domain wall in nanowires of varying thickness on SOT driven domain wall motion. We found large velocity asymmetries between Bloch chiralities near the current density required for reversal of the Bloch component of the magnetization and linked these asymmetries to a gradual reorientation of the domain wall structure which drives a non-negligible, chiral Néel component of the domain wall. We further explored the influence of saturation magnetization, film thickness, the Dzyaloshinskii-Moriya interaction, and in-plane fields on domain wall dynamics. These results provide a framework for the development of SOT based devices based on domain wall motion in nanowires beyond the ultrathin film limit.

Keywords: nanomagnetism; micromagnetism; spintronics; spin-orbit torques; thin film magnetism

Citation: Staggers, T.L.; Pollard, S.D. Dynamic Bloch Chirality and Enhanced Velocities from Spin-Orbit Torque Driven Domain Wall Motion in Thick Magnetic Films. *Magnetochemistry* **2022**, *8*, 119. https://doi.org/10.3390/magnetochemistry8100119

Academic Editor: José Vergara

Received: 18 September 2022
Accepted: 3 October 2022
Published: 6 October 2022

1. Introduction

The propagation of magnetic domain walls under the influence of spin polarized currents has garnered intense interest due to its potential applications in a variety of spintronic memory, logic, and sensing devices [1–8] as well as the intriguing fundamental physics governing the interaction of spin currents with magnetization [9–14]. Traditionally, current induced motion has been explored in magnetic states wherein the static domain wall structure may be described as fully Bloch or Néel-like. In ultrathin films with a strong Dzyaloshinskii-Moriya interaction (DMI) driven by symmetry breaking at interfaces, for example, a Néel domain wall may form [15–17]. This Néel structure allows field-free current driven domain wall motion while enhancing domain wall velocities and suppressing the Walker breakdown field [18]. In films without DMI, a Bloch structure is favorable, and, without an in-plane symmetry breaking field, domain wall motion is suppressed [19–22].

In magnetic films with perpendicular anisotropy, no DMI, and a film thickness greater than the exchange length, however, domain walls cannot be characterized as purely Bloch or Néel, and instead the competition of exchange and demagnetization energies results in a flux closure state, with Néel caps forming at the surfaces with an achiral central Bloch component [23–27], as shown in Figure 1. The sense of rotation of the Néel caps across the domain wall boundary is determined by the relative orientation of the magnetization on each side of the domain wall. For moderate DMI, the Néel cap corresponding to the chirality energetically preferred by the DMI will be enhanced, with the energetically unfavorable Néel cap suppressed. These non-uniform structures play a key role in current driven magnetization dynamics. For instance, this structure modifies the skyrmion Hall

angle during current driven skyrmion motion and allows for enhanced or suppressed velocities depending on the specific current injection geometry, even in the absence of DMI [25,26,28,29]. Further, the spin current itself can result in modified domain wall structure, leading to current density dependent dynamics and current driven switching of the Bloch component of the magnetization [30]. However, the role of this structure and its interaction with spin currents on current induced domain wall motion in thick, perpendicularly magnetized nanotracks has been largely unexplored.

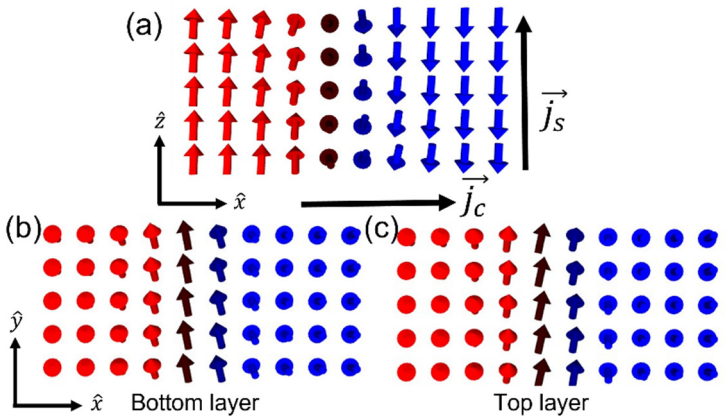

Figure 1. Schematic of a mixed Bloch/Néel domain wall without DMI. (**a**) Cross section view of the spin structure in the x–z plane of a thick ferromagnetic film with perpendicular anisotropy showing the central Bloch component with twisting near the surfaces indicative of the formation of Néel caps. The direction of charge and spin currents are noted by $\vec{j_c}$ and $\vec{j_s}$, respectively, while the spin polarization is orthogonal to both $\vec{j_c}$ and $\vec{j_s}$. (**b**,**c**) Bottom and top surfaces of the film, respectively, in the x–y planes demonstrating the clear deviation from a pure Bloch structure and the varied chirality of the Néel caps at each surface.

In this work, we use micromagnetic simulations to understand the reorientation process in thick magnetic films during application of spin polarized currents and the corresponding domain wall motion as a function of injection geometry, film thickness, current density, and saturation magnetization. We found that, for Bloch chiralities aligned antiparallel to the spin current polarization direction, the domain wall first reorients with a chiral Néel component resulting in an increased propagation velocity near the spin current required for domain wall reorientation, even in the absence of DMI or an applied in-plane field. The maximum velocity and required current density for switching the Bloch chirality may be controlled via application of an in-plane field, either parallel or orthogonal to the wire long axis. We further explored the combined effects of this current driven reorientation and moderate DMI.

2. Methods

Micromagnetic modelling of domain wall velocities in a nanowire was carried out using MuMax3 [31,32]. The nanowire geometry was chosen with dimensions of 1024 nm × 128 nm × t, where t is the film thickness in nanometers with a mesh of 512 × 128 × N cells and N varied from 1 to 10. Unless stated otherwise, t = 10 nm with N = 5. Material parameters were chosen to be consistent with standard Co-based multilayers and alloys [1,33–35]. The saturation magnetization, M_s, was set to 400 kA/m unless otherwise stated. For all simulations, we used a damping $\alpha = 0.1$, an exchange stiffness $A_{ex} = 10$ pJ/m, and a uniaxial anisotropy $K_u = 4.0 \times 10^5$ J/m^3. For $M_s = 400$ kA/m, this corresponds to an exchange length l_{ex} of nominally 10 nm, where $l_{ex} = \sqrt{2A_{ex}/\mu_0 M_s^2}$ and $\mu_0 = 4\pi \times 10^{-7}$ H/m is the vacuum permeability. We note that, for realistic films, the anisotropy may vary significantly with the film thickness, and more work needs to be carried out in order to better understand the potential effect this may have in determining

the specific domain velocity scaling of the geometries studied in this work. The nanowire was initialized and relaxed in a two-domain state, with the magnetization pointing in the positive z-direction to the left of the domain wall and in the negative z-direction to the right of the domain wall. The central Bloch component of the domain wall was chosen to lie along the positive y-direction or negative y-direction, wherein wires with central Bloch magnetization along the positive and negative y-directions are denoted as $M_Y = 1$ and $M_Y = -1$ respectively. The system was then allowed to relax at zero magnetic field and without any applied currents to obtain the initial magnetization state. The current density, $\vec{j}$, was modeled as a vertical current fully spin polarized along the y-axis. Note that only damping-like torques, which can originate from the spin Hall effect and current flowing along the x-direction, were considered in this work. The spin current was modeled as uniform across the film thickness, as is the case for bulk spin orbit torques (SOTs) recently found in a variety of ferro- and ferrimagnetic multilayers and alloys [14,35,36]. To exclude edge effects during domain wall motion, the simulation window was dynamically shifted such that the domain wall remained in the center, approximating an infinitely long wire. An example simulation file is included as a Supplementary File S1. As the damping-like term acts to align the magnetization along the spin polarization direction [30], large current densities will align the Bloch component of the magnetization along the spin polarization direction. As such, near the reorientation current density, a dynamic step size in current density was used with measuring domain wall velocities as a function of current density, with a step size of 2×10^9 A/m^2 immediately prior to reversal. This allows for a better capture of the maximum domain wall velocities near the critical current density. For the simulations carried in this work, a step size on the order of 1×10^{-13} s was used, corresponding to roughly 500,000 total steps per velocity measurement. Results are also compared to thin films with a weak DMI of $|D| = 50$ μJ/m^2 throughout the film thickness, comparable to recently discovered bulk DMI in a variety of ferro- and ferrimagnetic alloys [33,35,37]. All simulations were carried out at 0 K, unless otherwise noted. In simulations at non-zero temperatures, a temperature of 300 K is implemented by modelling the temperature as an effective fluctuating thermal field [31,38].

3. Results and Discussion

As shown in Figure 2, at large current densities, only a single Bloch chirality is stable due to realignment of the domain wall along the spin polarization direction. The chirality is determined by the current spin polarization direction, and the velocity for both chiralities is negative with a speed of a few m/s. However, at low current densities, both Bloch chiralities are stable. In the case wherein the Bloch component of the domain wall is aligned antiparallel to the current polarization direction, a sharp increase of the domain wall velocity is observed up to the current required for chirality reversal. For the 10 nm thick film with $M_s = 400$ kA/m, the velocity reaches 25.6 m/s at a current density of 58×10^9 A/m^2 prior to Bloch reversal at 60×10^9 A/m^2, when the central Bloch component is aligned antiparallel to the spin polarization, compared to a velocity of -1.7 m/s observed for the Bloch magnetization parallel to the spin polarization direction at equal current densities. This significant enhancement of velocity is achieved at moderate current densities, in line with experimentally accessible injection schemes. For example, assuming a spin Hall angle of 0.1, typical of heavy metals such as Pt, this would correspond to a true injection current density of 5.8×10^{11} A/m^2, which has been previously achieved in a variety of switching measurements.

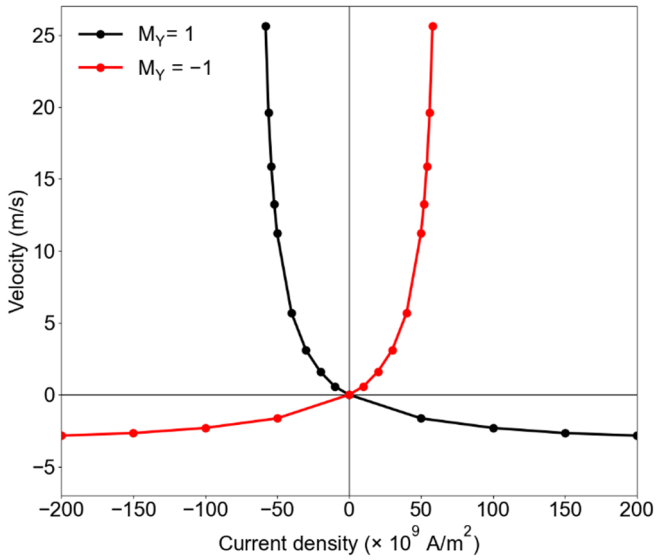

Figure 2. Velocity vs. current density for both Bloch chiralities in a 10 nm thick, $M_s = 400$ kA/m magnetic film. Saturation of negative velocities at high current densities are clearly observed, as well as the enhanced velocity in proximity to current densities required for reversal of the domain wall magnetization, nominally $\left|\vec{j}\right| = 58 \times 10^9$ A/m^2.

For thinner films, this asymmetry is weaker, and disappears entirely in the ultrathin limit. For a 2 nm thick film, no velocity was observed for either chirality, even at large current densities. This is in line with previous predictions in ultrathin films, wherein an in-plane field is necessary in order to induce motion. For thicker films, greater maximum velocities were observed, as shown in Figure 3a. The motion for low thicknesses is in line with previous reports showing that, without DMI, an in-plane field is required to induce domain wall motion [34,35,39]. The enhanced domain wall velocity further scales with saturation magnetization, which necessitates larger current densities for high saturation magnetization and lower current densities for lower saturation magnetizations, as shown in Figure 3b.

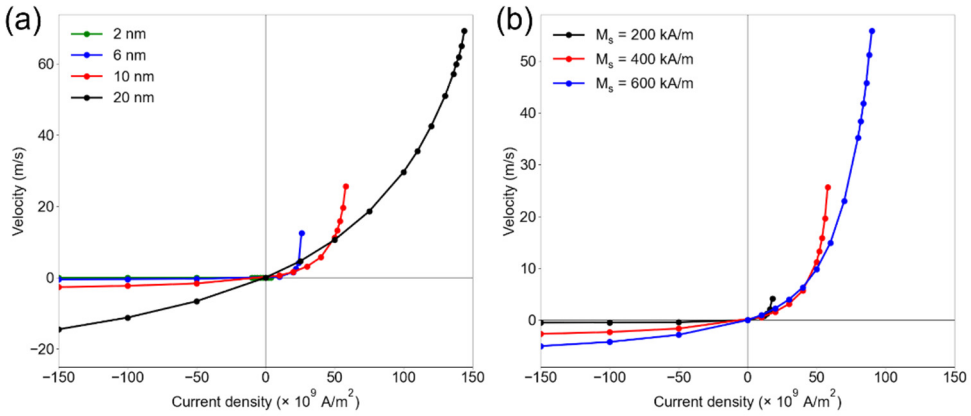

Figure 3. Velocity vs. current density for varying (**a**) t and (**b**) M_s. Increasing t or M_s result in larger maximum velocities and increased current densities necessary for switching. Results are shown for $M_Y = -1$.

The scaling of velocity in thick magnetic films may be qualitatively understood via modifications to the domain wall structure due to the spin polarized current, as shown in Figures 4 and 5. For a static domain wall, the thickness averaged component of the magnetization along the wire long axis is $M_x = 0$ due to the symmetric nature of the

Néel caps at top and bottom surfaces, as previously shown in Figure 1. As the domain driving current increases, the transition from one Bloch chirality to another begins with the gradual reorientation of the magnetization through a mixed Bloch/Néel state. This results in an increase in domain wall velocity due to the interaction of the spin current with the increasing Néel component of the magnetization. The direction of the rotation depends on the direction of the spin current and the Bloch chirality of the domain wall. This rotation is most pronounced at the wire edge as compared to the central portion of the wire and leads to switching propagating from the wire edge inward.

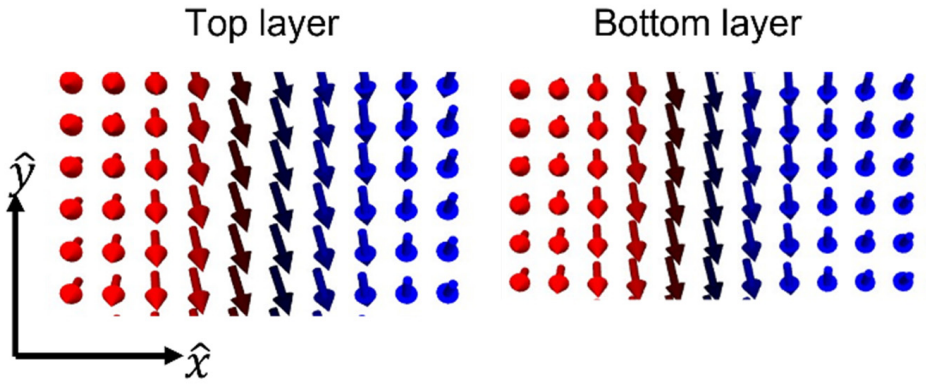

Figure 4. Domain wall structure at both top and bottom simulation cells at a current density of 58 kA/m^2, immediately prior to reversal of the $M_y = -1$ domain wall.

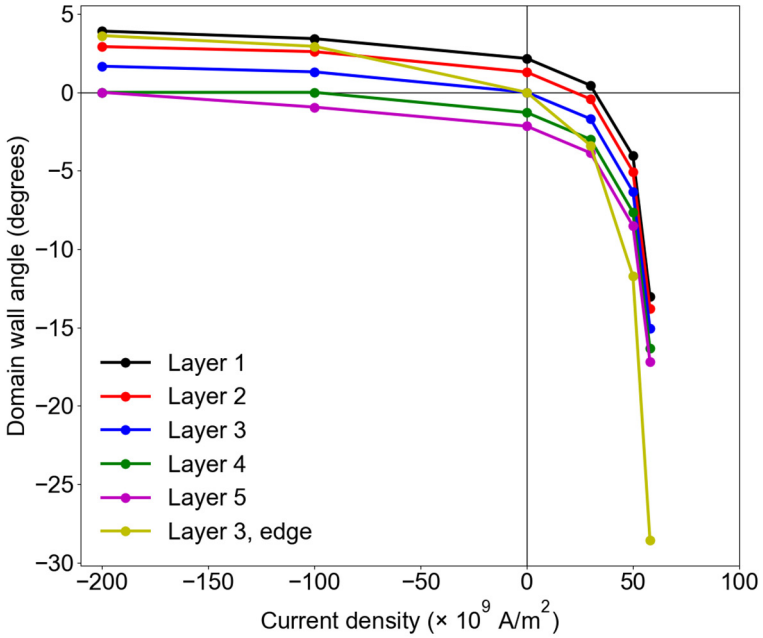

Figure 5. Domain wall angle as a function of current density taken for different simulation layers, wherein layer describes the cell layer number, with layer 1 referring to the bottom of the wire geometry, and 5 corresponding to the top of the wire geometry. Unless otherwise noted, the domain wall angle is determined by the maximum rotation away from a purely Bloch domain wall, with a positive value denoting a clockwise rotation, and counterclockwise negative, along the center of the wire. Data for the domain wall angle at the edge of the wire are also shown. Results are shown for $M_Y = -1$.

Simulations using an effective thermal field with a temperature of 300 K were carried out to ensure the asymmetric motion was preserved at realistic temperatures. Thermal fluctuations will result in local variations in the domain wall structure, which will modify the domain wall velocity. This leads to variations in the domain wall velocity as a function

of time, as seen in Figure 6. However, over time scales of 100 ns, the drastic asymmetries are preserved, with a sharp increase in the domain wall displacement with a current density of -50×10^9 A/m^2 relative to current densities further from the critical current density for switching of the Bloch component of the domain wall.

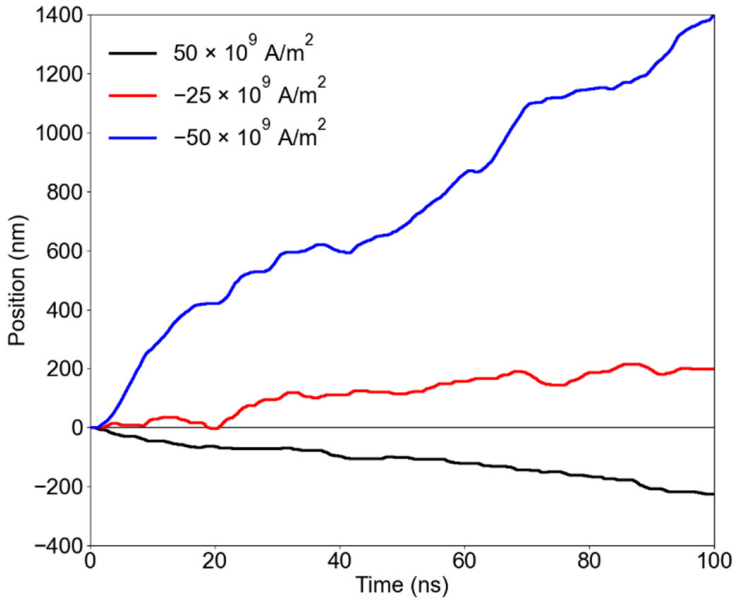

Figure 6. Domain wall displacement as a function of time with a temperature of 300 K. Variations of the domain wall velocity are due to thermal fluctuations of the domain wall structure. Data are shown for $M_Y = 1$.

To understand the influence of external fields on domain wall motion, external magnetic fields were applied either parallel (longitudinal) or orthogonal (transverse) to the wire's long-axis. The longitudinal field lies along the x-axis while the transverse field lies along the y-axis, as described in Figure 1b. A transverse magnetic field aligned parallel to the domain wall can be used to either enhance the required current density for switching of the Bloch component of the domain wall when the field is applied parallel to the Bloch component or decrease the required current density when applied antiparallel to the Bloch component, i.e., when the field is applied 180 degrees from the Bloch component of the domain wall. As shown in Figure 7a, the field parallel to the Bloch component results in a larger velocity achieved prior to switching, at the tradeoff of a larger required current density for the onset of velocity enhancements due to the suppressed Néel component of the wall at lower current densities. For a field of 40 mT applied antiparallel to the Bloch magnetization, a velocity of 2.6 m/s is achieved immediately below the switching current density at 12×10^9 A/m^2. For the field applied parallel to the Bloch component, but opposite the spin current polarization, the necessary current density for switching increases to 102×10^9 A/m^2 with a maximum velocity of 61.7 m/s. This suggests potential use of transverse fields to either reduce the required currents necessary to achieve enhanced velocities, or to increase maximal velocities at the expense of higher required current densities.

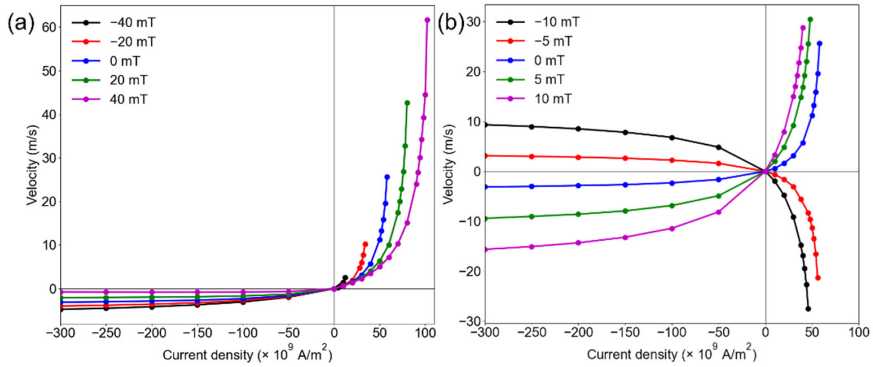

Figure 7. Velocity vs. current density for (**a**) a field applied along the y-axis orthogonal to the wire and (**b**) applied parallel to the wire. All data are shown for an initial $M_y = -1$ Bloch chirality.

For a field applied along the nanowire, shown in Figure 7b, the field results in a rotation of the domain wall magnetization along the applied field direction, which results in a sign change in velocity for negative applied fields [40]. The asymmetric change in velocities is a result of this rotation either adding to or subtracting from the intrinsic dynamic Néel chirality determined by the initial Bloch chirality, as shown in Figure 4. The in-plane field also results in a decrease of the current density required to switch the Bloch chirality. This is most pronounced for fields applied parallel to the intrinsically favored dynamic Néel chirality.

The influence of DMI on domain wall velocity is shown in Figure 8. As expected, the velocities at large current densities are significantly enhanced compared to the case without DMI. This is a result of the partial alignment of the domain wall towards a Néel wall due to the DMI effective field. The magnitude of the velocities for positive and negative current densities are not equal due to either enhancement or suppression of the Néel component of the domain wall, as determined by the sign and magnitude of the DMI [16]. For low current densities, an achiral Bloch component persists provided the DMI is not too strong. This Bloch component behaves similarly to that without DMI, however with a smaller extent due to the rotation of the domain wall towards Néel-type [25,26,28]. Of note, the current required to switch the Bloch component along the polarization direction of the current is lower than that obtained for no DMI. Further, the velocity difference between opposite Bloch chiralities is lower compared to the asymmetries at low fields observed in Figure 2, and no sign change in the direction of domain wall propagation upon reversal of the Bloch component was observed, as previously seen for domain walls in ultrathin films with DMI [40].

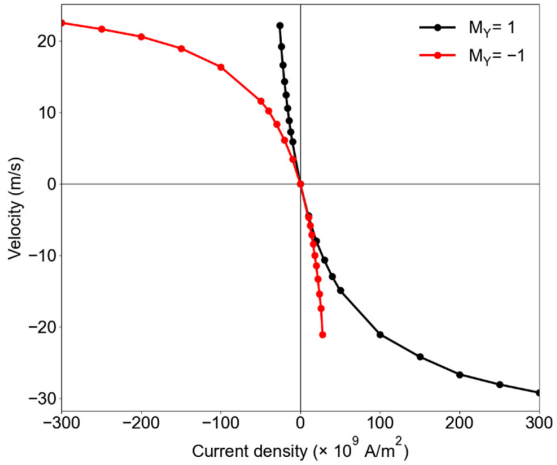

Figure 8. Velocity vs. current density for $D = 50$ μJ/m^2 and opposing Bloch chiralities of the domain wall.

4. Conclusions

We investigated the SOT driven dynamics of domain walls in thick ferromagnetic films, wherein competition between demagnetization and exchange energies result in a mixed Bloch-Néel domain wall structure. We found the Bloch component of the domain wall can strongly influence domain wall dynamics, leading to enhanced velocities even without an applied in-plane field or DMI at low current densities, and unidirectional motion at high current densities. This is explained via the rotation of the domain wall magnetization towards a Néel structure, before switching to align with the applied spin current. The velocities obtained in this work near the transition current density, even without the presence of DMI, are on the same order of those found for magnetic skyrmions in thick multilayers [25,41] and in TbCoFe wires [42] with DMI. These effects can be modified through application of in-plane magnetic fields and persist with the presence of weak DMI. These findings deviate from standard models of ultrathin films and provide a framework for the development of spintronic devices utilizing ferromagnetic films with thicknesses greater than the exchange length and generating bulk spin-orbit torques.

Supplementary Materials: The following supporting information can be downloaded at: https://www.mdpi.com/article/10.3390/magnetochemistry8100119/s1, File S1: Supplementary 1.

Author Contributions: Conceptualization, T.L.S. and S.D.P.; methodology, T.L.S. and S.D.P.; formal analysis, T.L.S. and S.D.P.; investigation, T.L.S. and S.D.P.; resources, S.D.P.; data curation, T.L.S.; writing—original draft preparation, S.D.P.; writing—review and editing, T.L.S.; visualization, T.L.S. and S.D.P.; supervision, S.D.P.; funding acquisition, S.D.P. All authors have read and agreed to the published version of the manuscript.

Funding: The authors acknowledge financial support from the National Science Foundation through award NSF-ECCS 2138271.

Institutional Review Board Statement: Not applicable.

Informed Consent Statement: Not applicable.

Data Availability Statement: Data used in this work are available upon request from the corresponding author.

Conflicts of Interest: The authors declare no conflict of interest.

References

1. You, L.; Sousa, R.C.; Bandiera, S.; Rodmacq, B.; Dieny, B. Co/Ni Multilayers with Perpendicular Anisotropy for Spintronic Device Applications. *Appl. Phys. Lett.* **2012**, *100*, 172411. [CrossRef]
2. Pribiag, V.S.; Krivorotov, I.N.; Fuchs, G.D.; Braganca, P.M.; Ozatay, O.; Sankey, J.C.; Ralph, D.C.; Buhrman, R.A. Magnetic Vortex Oscillator Driven by d.c. Spin-Polarized Current. *Nat. Phys.* **2007**, *3*, 498–503. [CrossRef]
3. Moriyama, T.; Zhou, W.; Seki, T.; Takanashi, K.; Ono, T. Spin-Orbit-Torque Memory Operation of Synthetic Antiferromagnets. *Phys. Rev. Lett.* **2018**, *121*, 167202. [CrossRef] [PubMed]
4. Fan, Y.; Han, X.; Zhao, X.; Dong, Y.; Chen, Y.; Bai, L.; Yan, S.; Tian, Y. Programmable Spin-Orbit Torque Multistate Memory and Spin Logic Cell. *ACS Nano* **2022**, *16*, 6878–6885. [CrossRef] [PubMed]
5. Sato, N.; Xue, F.; White, R.M.; Bi, C.; Wang, S.X. Two-Terminal Spin–Orbit Torque Magnetoresistive Random Access Memory. *Nat. Electron.* **2018**, *1*, 508–511. [CrossRef]
6. Kim, Y.; Fong, X.; Kwon, K.W.; Chen, M.C.; Roy, K. Multilevel Spin-Orbit Torque MRAMs. *IEEE Trans. Electron. Devices* **2015**, *62*, 561–568. [CrossRef]
7. De Orio, R.L.; Ender, J.; Fiorentini, S.; Goes, W.; Selberherr, S.; Sverdlov, V. Optimization of a Spin-Orbit Torque Switching Scheme Based on Micromagnetic Simulations and Reinforcement Learning. *Micromachines* **2021**, *12*, 443. [CrossRef]
8. Yang, S.; Tan, M.; Yu, T.; Li, X.; Wang, X.; Zhang, J. Hybrid Reduced Graphene Oxide with Special Magnetoresistance for Wireless Magnetic Field Sensor. *Nanomicro Lett.* **2020**, *12*, 69. [CrossRef] [PubMed]
9. Woo, S.; Song, K.M.; Zhang, X.; Zhou, Y.; Ezawa, M.; Finizio, S.; Raabe, J.; Choi, J.W.; Min, B.-C.; Koo, H.C.; et al. Current-Driven Dynamics and Inhibition of the Skyrmion Hall Effect of Ferrimagnetic Skyrmions in GdFeCo Films. *Nat. Commun.* **2018**, *9*, 959. [CrossRef] [PubMed]
10. Jiang, W.; Zhang, X.; Yu, G.; Zhang, W.; Jungfleisch, M.B.; Pearson, J.E.; Heinonen, O.; Wang, K.L.; Zhou, Y.; Hoffmann, A.; et al. Direct Observation of the Skyrmion Hall Effect. *Nat. Phys.* **2016**, *13*, 162. [CrossRef]

11. Kanazawa, N.; Kubota, M.; Tsukazaki, A.; Kozuka, Y.; Takahashi, K.S.; Kawasaki, M.; Ichikawa, M.; Kagawa, F.; Tokura, Y. Discretized Topological Hall Effect Emerging from Skyrmions in Constricted Geometry. *Phys. Rev. B* **2015**, *91*, 041122. [CrossRef]
12. Wang, Y.; Zhu, D.; Wu, Y.; Yang, Y.; Yu, J.; Ramaswamy, R.; Mishra, R.; Shi, S.; Elyasi, M.; Teo, K.-L.; et al. Room Temperature Magnetization Switching in Topological Insulator-Ferromagnet Heterostructures by Spin-Orbit Torques. *Nat. Commun.* **2017**, *8*, 1364. [CrossRef] [PubMed]
13. Wang, Y.; Zhu, D.; Yang, Y.; Lee, K.; Mishra, R.; Go, G.; Oh, S.; Kim, D.; Cai, K.; Liu, E.; et al. Magnetization Switching by Magnon-Mediated Spin Torque through an Antiferromagnetic Insulator. *Science* **2019**, *366*, 1125–1128. [CrossRef] [PubMed]
14. Yu, J.; Bang, D.; Mishra, R.; Ramaswamy, R.; Oh, J.H.; Park, H.-J.; Jeong, Y.; van Thach, P.; Lee, D.-K.; Go, G.; et al. Long Spin Coherence Length and Bulk-like Spin–Orbit Torque in Ferrimagnetic Multilayers. *Nat. Mater.* **2019**, *18*, 29–34. [CrossRef]
15. Benitez, M.J.; Hrabec, A.; Mihai, P.; Moore, T.; Burnell, G.; McGrouther, D.; Marrows, C.H.; McVitie, S. Magnetic Microscopy and Topological Stability of Homochiral Néel Domain Walls in a Pt/Co/AlOx Trilayer. *Nat. Commun.* **2015**, *6*, 8957. [CrossRef] [PubMed]
16. Hrabec, A.; Porter, N.A.; Wells, A.; Benitez, M.J.; Burnell, G.; McVitie, S.; McGrouther, D.; Moore, T.A.; Marrows, C.H. Measuring and Tailoring the Dzyaloshinskii-Moriya Interaction in Perpendicularly Magnetized Thin Films. *Phys. Rev. B* **2014**, *90*, 020402. [CrossRef]
17. Yoshimura, Y.; Kim, K.J.; Taniguchi, T.; Tono, T.; Ueda, K.; Hiramatsu, R.; Moriyama, T.; Yamada, K.; Nakatani, Y.; Ono, T. Soliton-like Magnetic Domain Wall Motion Induced by the Interfacial Dzyaloshinskii–Moriya Interaction. *Nat. Phys.* **2015**, *12*, 157–161. [CrossRef]
18. Thiaville, A.; Rohart, S.; Jué, É.; Cros, V.; Fert, A. Dynamics of Dzyaloshinskii Domain Walls in Ultrathin Magnetic Films. *Europhys. Lett.* **2012**, *100*, 57002. [CrossRef]
19. Liu, L.; Lee, O.J.; Gudmundsen, T.J.; Ralph, D.C.; Buhrman, R.A. Current-Induced Switching of Perpendicularly Magnetized Magnetic Layers Using Spin Torque from the Spin Hall Effect. *Phys. Rev. Lett.* **2012**, *109*, 096602. [CrossRef]
20. Miron, I.M.; Garello, K.; Gaudin, G.; Zermatten, P.J.; Costache, M.; Auffret, S.; Bandiera, S.; Rodmacq, B.; Schuhl, A.; Gambardella, P. Perpendicular Switching of a Single Ferromagnetic Layer Induced by In-Plane Current Injection. *Nature* **2011**, *476*, 189–193. [CrossRef]
21. Liu, L.; Pai, C.F.; Li, Y.; Tseng, H.W.; Ralph, D.C.; Buhrman, R.A. Spin-Torque Switching with the Giant Spin Hall Effect of Tantalum. *Science* **2012**, *336*, 555–558. [CrossRef] [PubMed]
22. Estevez, G.; Cui, B.; Zhu, Z.; Wu, C.; Guo, X.; Nie, Z.; Wu, H.; Guo, T.; Chen, P.; Zheng, D.; et al. Comprehensive Study of the Current-Induced Spin-Orbit Torque Perpendicular Effective Field in Asymmetric Multilayers. *Nanomaterials* **2022**, *12*, 1887. [CrossRef]
23. Montoya, S.A.; Couture, S.; Chess, J.J.; Lee, J.C.T.; Kent, N.; Im, M.Y.; Kevan, S.D.; Fischer, P.; McMorran, B.J.; Roy, S.; et al. Resonant Properties of Dipole Skyrmions in Amorphous Fe/Gd Multilayers. *Phys. Rev. B* **2017**, *95*, 224405. [CrossRef]
24. Montoya, S.A.; Couture, S.; Chess, J.J.; Lee, J.C.T.; Kent, N.; Henze, D.; Sinha, S.K.; Im, M.-Y.; Kevan, S.D.; Fischer, P.; et al. Tailoring Magnetic Energies to Form Dipole Skyrmions and Skyrmion Lattices. *Phys. Rev. B* **2017**, *95*, 024415. [CrossRef]
25. Legrand, W.; Chauleau, J.-Y.; Maccariello, D.; Reyren, N.; Collin, S.; Bouzehouane, K.; Jaouen, N.; Cros, V.; Fert, A. Hybrid Chiral Domain Walls and Skyrmions in Magnetic Multilayers. *Sci. Adv.* **2018**, *4*, eaat0415. [CrossRef]
26. Garlow, J.A.; Pollard, S.D.; Beleggia, M.; Dutta, T.; Yang, H.; Zhu, Y. Quantification of Mixed Bloch-Néel Topological Spin Textures Stabilized by the Dzyaloshinskii-Moriya Interaction in Co/Pd Multilayers. *Phys. Rev. Lett.* **2019**, *122*, 237201. [CrossRef]
27. Banerjee, C.; Gruszecki, P.; Klos, J.W.; Hellwig, O.; Krawczyk, M.; Barman, A. Magnonic Band Structure in a Co/Pd Stripe Domain System Investigated by Brillouin Light Scattering and Micromagnetic Simulations. *Phys. Rev. B* **2017**, *96*, 024421. [CrossRef]
28. Chauleau, J.-Y.; Legrand, W.; Reyren, N.; Maccariello, D.; Collin, S.; Popescu, H.; Bouzehouane, K.; Cros, V.; Jaouen, N.; Fert, A. Chirality in Magnetic Multilayers Probed by the Symmetry and the Amplitude of Dichroism in X-Ray Resonant Magnetic Scattering. *Phys. Rev. Lett.* **2018**, *120*, 037202. [CrossRef]
29. Pollard, S.D.; Garlow, J.A.; Kim, K.W.; Cheng, S.; Cai, K.; Zhu, Y.; Yang, H. Bloch Chirality Induced by an Interlayer Dzyaloshinskii-Moriya Interaction in Ferromagnetic Multilayers. *Phys. Rev. Lett.* **2020**, *125*, 227203. [CrossRef]
30. Yoon, J.; Lee, S.W.; Kwon, J.H.; Lee, J.M.; Son, J.; Qiu, X.; Lee, K.J.; Yang, H. Anomalous Spin-Orbit Torque Switching Due to Field-like Torque–Assisted Domain Wall Reflection. *Sci. Adv.* **2017**, *3*, e1603099. [CrossRef]
31. Vansteenkiste, A.; Leliaert, J.; Dvornik, M.; Helsen, M.; Garcia-Sanchez, F.; van Waeyenberge, B. The Design and Verification of MuMax3. *AIP Adv.* **2014**, *4*, 107133. [CrossRef]
32. Vansteenkiste, A.; de Wiele, B. van MUMAX: A New High-Performance Micromagnetic Simulation Tool. *J. Magn. Magn. Mater.* **2011**, *323*, 2585–2591. [CrossRef]
33. Kim, D.H.; Haruta, M.; Ko, H.W.; Go, G.; Park, H.J.; Nishimura, T.; Kim, D.Y.; Okuno, T.; Hirata, Y.; Futakawa, Y.; et al. Bulk Dzyaloshinskii–Moriya Interaction in Amorphous Ferrimagnetic Alloys. *Nat. Mater.* **2019**, *18*, 685–690. [CrossRef]
34. Zheng, Z.; Zhang, Y.; Lopez-Dominguez, V.; Sánchez-Tejerina, L.; Shi, J.; Feng, X.; Chen, L.; Wang, Z.; Zhang, Z.; Zhang, K.; et al. Field-Free Spin-Orbit Torque-Induced Switching of Perpendicular Magnetization in a Ferrimagnetic Layer with a Vertical Composition Gradient. *Nat. Commun.* **2021**, *12*, 4555. [CrossRef]
35. Xie, X.; Zhao, X.; Dong, Y.; Qu, X.; Zheng, K.; Han, X.; Han, X.; Fan, Y.; Bai, L.; Chen, Y.; et al. Controllable Field-Free Switching of Perpendicular Magnetization through Bulk Spin-Orbit Torque in Symmetry-Broken Ferromagnetic Films. *Nat. Commun.* **2021**, *12*, 2473. [CrossRef] [PubMed]

36. Jamali, M.; Narayanapillai, K.; Qiu, X.; Loong, L.M.; Manchon, A.; Yang, H. Spin-Orbit Torques in Co/Pd Multilayer Nanowires. *Phys. Rev. Lett.* **2013**, *111*, 246602. [CrossRef] [PubMed]
37. Zhang, Q.; Liang, J.; Bi, K.; Zhao, L.; Bai, H.; Cui, Q.; Zhou, H.A.; Bai, H.; Feng, H.; Song, W.; et al. Quantifying the Dzyaloshinskii-Moriya Interaction Induced by the Bulk Magnetic Asymmetry. *Phys. Rev. Lett.* **2022**, *128*, 167202. [CrossRef]
38. Brown, W.F. Thermal Fluctuations of a Single-Domain Particle. *J. Appl. Phys.* **2004**, *34*, 1319. [CrossRef]
39. Oh, Y.-W.; Chris Baek, S.; Kim, Y.M.; Lee, H.Y.; Lee, K.-D.; Yang, C.-G.; Park, E.-S.; Lee, K.-S.; Kim, K.-W.; Go, G.; et al. Field-Free Switching of Perpendicular Magnetization through Spin–Orbit Torque in Antiferromagnet/Ferromagnet/Oxide Structures. *Nat. Nanotechnol.* **2016**, *11*, 878–884. [CrossRef] [PubMed]
40. Ryu, K.-S.; Thomas, L.; Yang, S.-H.; Parkin, S. Chiral Spin Torque at Magnetic Domain Walls. *Nat. Nanotechnol.* **2013**, *8*, 527–533. [CrossRef] [PubMed]
41. Litzius, K.; Leliaert, J.; Bassirian, P.; Rodrigues, D.; Kromin, S.; Lemesh, I.; Zazvorka, J.; Lee, K.J.; Mulkers, J.; Kerber, N.; et al. The Role of Temperature and Drive Current in Skyrmion Dynamics. *Nat. Electron.* **2020**, *3*, 30–36. [CrossRef]
42. Ngo, D.T.; Ikeda, K.; Awano, H. Direct Observation of Domain Wall Motion Induced by Low-Current Density in TbFeCo Wires. *Appl. Phys. Express* **2011**, *4*, 093002. [CrossRef]